Design, Fabrication, and Validation of a New Family of 3D-Printable Structurally-Programmable Actuators for Soft Robotics

Ahmed Altelbani, Haoran Zhou , Sarmad Mehrdad, *Student Member, IEEE*, Farshid Alambeigi, *Member, IEEE*, and S. Farokh Atashzar, *Member, IEEE*

***Abstract*—Soft robots have shown great potential for manufacturing exoskeletons, prostheses, and surgical robots. In this paper, we propose the concept of programmable soft robotics and will experimentally evaluate the performance in the context of continuum mechanisms. The proposed novel concept is motivated by the mechanical shape of RNA molecules which has a single-stranded polymeric molecule with a sugar-phosphate backbone and nitrogenous bases. The shape of the RNA and the type, location, and characteristics of the bases define the coded information. Due to the complexity of RNA, the proposed robot cannot be considered a "bio-inspired" design. Instead, we indirectly utilize the concept of encoding sequences and introduce a new family of soft continuum robots based on a novel design of 3D printable "mechanical library" and "embedded functions" to be implemented on the backbone structure for mechanical programming. Through structural coding of the bases, the paper proposed a wide range of continuum robots. The system has the potential to be scaled up for multiple degrees of freedom (DOF), while the dexterity and range can be structurally programmed. A set of three soft continuum systems are designed, simulated, manufactured. The performance is evaluated by comparing simulations and experiments. We observed that actuators have different hysteresis ranging from 7.50% to 38.36% (on average) with a standard deviation ranging from 5.56% to 40.72%. The results highlight the effect of inherent pneumatic delay causing the hysteresis loops, which should be considered for control.**

***Index Terms*—Exoskeletons, human-robot interaction, medical robotics, rehabilitation robotics, soft robotics.**

I. Introduction

SOFT robots have attracted a great deal of interest due to their unique characteristics, i.e., flexibility, safety, and adaptability [1]–[3]. One of the most common uses of soft actuators is rehabilitation robots [4] (in the format of soft exoskeletons [5]) and prosthetic technologies (in the format of soft bionic limbs [6]). Initial designs of soft robotic systems were made based on multi-step silicon molding [7], combined with some format of mechanical reinforcement such as fabrics (examples can be found in [8]–[11], and references therein). Although this method has shown high efficacy, the manufacturing process can be time-consuming, require complex molding and manual skills. Silicone molding is susceptible to a range of defects caused by human intervention and can be limited in terms of the achievable curvatures, DOF, and internal structure of the air chambers [12]. This would limit the scalability, repeatability, and possibly the efficacy of the system due to potential human errors during manufacturing [13]. Also, Silicon casting can be challenging in creating complex geometries, as it requires multi-phase fabrication processes "if realizable". Also, due to inconsistency and uncertainties during manual molding, the accuracy of computational and analytical models will be degraded [14]. This can challenge the control of soft robotic systems during complex tasks. An alternative approach that has recently been proposed is soft 3D printing, taking advantage of advanced additive manufacturing. Examples of 3D printable soft robotic systems can be found in [15]–[19].

In this paper, we capitalize on a recent surge to use 3D printing technologies and soft filament to generate soft robots. The method will (a) reduce uncertainties of manufacturing, (b) allow for generating complex internal geometries of air chambers, (c) enable the use of computational modeling, and (d) realize fast and accurate manufacturing and scaling. Thus, using 3D printers, it is possible to realize a wide range of complex soft mechanisms and extend the horizon of functionality for this technology [20]–[27], [27]–[30], [30], [31], [31], [32].

In this paper, we propose a new family of 3D-printable soft robots that allows for having multiple DOF, complex shapes, high-compliance, low cost, and high force-to-weight ratio. This actuator can be categorized as a multi-chambered multi-section actuator [33]. The structural programming of the proposed system is indirectly inspired by the polymetric structure of ribonucleic acid (RNA). The mechanical structure of RNA has a complex sugar-phosphate backbone connected to a variety of nitrogenous "bases". The particular complex molecular structure and types of bases encode the message and information

Manuscript received February 24, 2021; accepted July 13, 2021. Date of publication August 4, 2021; date of current version August 20, 2021. This material is based upon work supported by the US National Science Foundation under Grant No 2037878. *(Ahmed Altelbani, Haoran Zhou, and Sarmad Mehrdad contributed equally to this work.) (Corresponding author: S. Farokh Atashzar.)*

Ahmed Altelbani and Haoran Zhou are with the Department of Mechanical and Aerospace Engineering, New York University (NYU), Brooklyn, NY 11201 USA (e-mail: ama1059@nyu.edu; hz2206@nyu.edu).

Sarmad Mehrdad is with the Department of Electrical Computer Engineering, New York University (NYU), Brooklyn, NY 11201 USA (e-mail: sm9167@nyu.edu).

Farshid Alambeigi is with the Department of Mechanical Engineering, University of Texas at Austin, Austin USA (e-mail: farshid.alambeigi@austin.utexas.edu).

S. Farokh Atashzar is with the Department of Mechanical and Aerospace Engineering, New York University (NYU), Brooklyn, NY 11201 USA, and also with the Dept. of Electrical Computer Engineering, New York University (NYU), Brooklyn, NY 11201 USA (e-mail: f.atashzar@nyu.edu).

Digital Object Identifier 10.1109/LRA.2021.3101860

to be carried. Here, for the first time, and motivated by the mechanical architecture of RNA, we propose the programmable 3D printable soft robotic system, which can be coded using the proposed mechanical library in a way that behaves as instructed when activated. The proposed approach will introduce a new generation of soft continuum robotic systems, the shape of which can be finely programmed and embedded in the memory of the soft robot. In this paper, we introduce the main concept and functionalities of this new family of soft robots. The paper will show a variety of achievable memories for the shape of the robot. Using computer models, this work evaluates the functionality in experimental settings considering different shape capabilities, DOF, and dexterities.

The main contribution is to design, fabricate, and experimentally evaluate a new family of a 3D-printable soft robotic system, using sequential mechanical coding, that allows for having multiple DOF and several nonlinear shapes by implementing a mechanical library and embedded mechanical code which can be compiled by 3D Printing to generate a wide range of soft actuators. The "programmable" feature of the proposed framework allows us to generate various mechanisms by selectively fusing the proposed codes from the proposed mechanical library. The resulting actuator belongs to a wider class of soft robotic systems that have recently attracted a great deal of interest [24], [27], [27], [34]. In some literature, it is assumed that 3D Printing reduces the time, and complexity of fabrication, in addition to variability and susceptibility to human errors, when compared with silicone casting [26]. However, it should also be noted that the use of 3D Printing has some potential limitations and challenges, which should be considered when designing 3D printable soft actuators. Thus, it cannot be concluded that 3D printable soft robots are to replace traditional silicon-based robots. Several parameters should be considered, and the field can benefit from both methods. The main focus of this paper is to take a fundamental step ahead towards the systematic fabrication of Multi-DOF 3D printable soft actuators through the generation of a new mechanical library and embedded codes. This paper enables the development of a wide range of actuators using 3D printing technology. We also discuss the limitations (in Section III.C) to shed light on the future directions.

TABLE I
STRUCTURAL PROGRAMMING LIBRARY

Function	Description
Function#1	The density of the flexor and extensor bases
Function#2	The heterogeneous distribution of the flexor bases
Function#3	The heterogeneous distribution and location of the extensor bases with respect to the flexor bases
Function#4	The size, thickness, and rigidity of the inhibition link in between bases of any type (flexor/extensor)
Function#5	The thickness of the backbone
Function#6	The geometry of the air chamber activating the robot
Function#7	The isolation link decoupling multiple DOF (segments)
Function#8	The geometry and number of input channels for activating the soft robot

TABLE II
EMBEDDED MECHANICAL CODE

Code	Description
Code: {1}	Flexor bases
Code: {-1}	Extensor bases
Code: {0}	Flat (inactive) bases
Code: {+}	The isolation link (producing new DOF)
Code: {A| H or P}	Type of air chamber. P is for *Progressive* and H is for *Homogeneous*
Code: {B| H or P}	Type of backbone. P is for *Progressive* and H is for *Homogeneous*

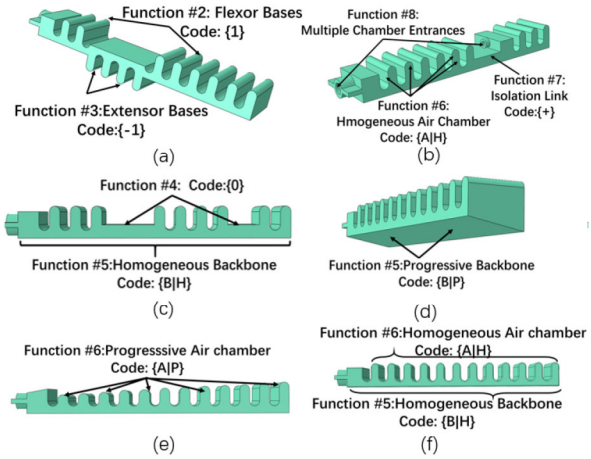

Fig. 1. Generic schematic & various functions of the library.

II. STRUCTURAL PROGRAMMING

The concept of 3D printable soft robots has recently attracted a great deal of interest [16], [34]–[38] and this paper proposes a new vision which can result in a systematic manufacturing process for complex soft robotic systems. The proposed actuator is made out of dented bellows and a backbone. The backbone can have one or more embedded air chambers (depending on the programmed DOF) connected to a subset of bellows, pressurizing of which results in bending of the actuator and generating the programmed shape with different intensity of actuation, depending on the deployed pressure in the corresponding chamber. This concept is indirectly inspired by the complex mechanical structure of RNA molecules. The geometry of the backbone is designed such that it resists elongation in the axial direction while distributing the pressure based on the programmed bases to generate a heterogeneous bending alongside the backbone. We propose two base functions for the soft actuators, i.e., flexor bases and extensor bases. The desired directionality, shape, DOF, dexterity, and power of the soft mechanism are coded using a novel mechanical programming library (given in Table I) and embedded mechanical codes (given in Table II). The library shows available behaviors which can be coded using embedded functions. Table I shows the programming function library. To elaborate on Function 1 in Table I, the flexor and extensor bases provide forward and backward bending of the actuator, respectively. Flexion is the downward bending when the air input is at the left, and extension is upward bending.

Fig. 1 shows an example schematic of the proposed soft continuum robot with annotated various sections associated with different programming functions, given in Table I. It should be noted that not all eight functions of the mechanical library

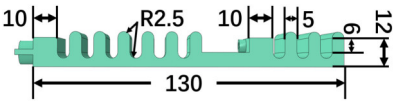

Fig. 2. Wall thickness and size of 2DOF actuator.

need to be used in one single actuator. The introduction of flexor-extensor active bases results in the possibility of non-homogeneous expansion of various sections of the robot, which introduces heterogeneous stress and strain, thus variable curvature alongside the robot. By changing the physical characteristics of the base, backbone, and air chamber, various distribution and actuation can be achieved. The actuators are capable of having multiple air chambers that can get activated separately and are isolated using isolation links. The isolation link results in activating various segments of the robot independently, while the inhibition link does not isolate the two air chambers but generates passive mechanical support for generating various shapes. Actuators can be designed by selecting and ordering the functions from the library. Thus, the mechanical coding is proposed in Table II for the functions explained in Table I.

III. Simulation and Experimental Implementation

In this section, three examples of the programmable robots proposed in the paper are discussed. It should be noted that in all actuators discussed in this paper, the spacing between all adjacent bases and the actuator's length is kept constant. In addition, the thickness of the sidewalls of the actuator is kept the same across all actuators (1.2 mm in thickness) since it provides a ground of comparison where the change in the actuator's behavior is solely due to the change in the mechanical coding (See Fig. 2).

A. FEM Simulation Settings

In order to verify the behavior of the actuators and avoid unfeasible design parameters before manufacturing, the Finite Element Method (FEM) of each design is utilized to simulate deformation during various levels of pressurizing for the three actuators.

- *Material selection and assignment:* The material used is created as a hyperplastic Ogden polynomial material with $N = 3,\ \alpha_1 = 0.508,\ \mu_1 = -30.921\,MPa,\ \alpha_2 = 1.375,\ \mu_2 = 10.342\,MPa, \alpha_3 = -0.482, \mu_3 = 26.791\,MPa.$
- *Surface assignment, step creation, boundary condition, and load assignment:* Surface sets (Up1, Up2, Bottom, Sides, Back, and Front) were created for each actuator to cover all cavity surfaces. Only one step was created with the static and general method. The ENCASTRE boundary condition was implemented at the air tube side of the actuator, and equally spaced 200 kPa pressure was applied to all six surface sets for two designed robots with one chamber. The third actuator designed has two independent air chambers generating 2 DOF.

TABLE III
Mechanical Code for the Models in Fig. 1

Model	Code	Given Name
(a)	{A| H, B| H: [1,1,-1,-1,-1,-1,1,1,1,1,1,1]}	S-shape
(b)	{A| H, B| H: [1,1,1,1,1,1,+,1,1,1]}	2DOF
(c)	{A| H, B| H: [1,1,1,0,0,0,1,1,1,1,0,1,1]}	Flat
(d)	{A| H, B| P: [1,1,1,1,1,1,1,1,1,1,1,1,1]}	HP-Original
(e)	{A| P, B| H: [1,1,1,1,1,1,1,1,1,1,1,1,1]}	PH-Original
(f)	{A| H, B| H: [1,1,1,1,1,1,1,1,1,1,1,1,1]}	HH-Original

TABLE IV
Printing Parameters for Different Slicing Methods

	Manual Vase-Mode	User-Defined
Nozzle Size	$0.4mm$	$0.4mm$
Layer Height	$0.1mm$	$0.1mm$
Printing Temperature	$235°C$	$230°C$
Bed Temperature	$60°C$	$60°C$
Printing Speed	$30mm/s$	$30mm/s$
Wall Thickness	$1.2mm$	N/A
Top/Bottom layer thickness	$1.2mm$	N/A
Infill	0%	100%
Retraction	Off	Off
Line Width	$0.4mm$	$0.4mm$

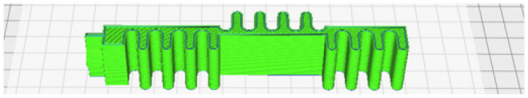

Fig. 3. Printing orientation on Cura.

- *Mesh:* In order to obtain computation efficiency, solid tetrahedral quadratic hybrid element C3D10H was applied with different global seed sizes to each model.

B. Design and Manufacturing Settings

The actuators are 3D printed using an Anycubic Mega X 3D printer and A85 Ninjaflex TPU flexible filament. The actuator was designed in CAD software and sliced using Cura 4.6. Two different concepts of slicing the 3D models were used, namely: (a) manual vase mode and (b) slicing using user-specified parameters [39]. Table IV shows the parameters used in the two tested 3D printing methods.

In order to minimize the printing time and maximize the quality, the actuators were printed on the side, Fig. 3. Due to the close proximity of the walls of each base, for printing the top layer, there is no need for any support material. Thus, placing the actuator in this orientation eliminates the need for the use of supporting material. Other orientations may cause the supporting material to be trapped in locations that cannot be accessed.

C. Challenges and Limitations

As mentioned earlier in the introduction, 3D Printing has expanded the horizon of manufacturing soft actuators. Fused Deposition Modeling (FDM) for printing flexible TPU filaments has made it possible to generate complex shapes using 3D printers without the need for multi-stepped silicon casting. In

some literature, 3D printing is motivated by the corresponding potential for the reduction of the time, and complexity of fabrication, in addition to possible less variability and susceptibility to human errors (please see [26] for more details). However, there are several limitations with the use of 3D printing methods which should be considered when deciding about the manufacturing technique for a robot. In this Section, we provide an overview of two possible limitations which may challenge manufacturing.

- *Challenge #1 - Moisture*: TPU filaments, which are often used for flexible Printing, are highly hygroscopic and tend to absorb moisture from the ambient air if not properly maintained. The absorbed moisture will disrupt the printing process and results in micro-holes in the walls of the actuators. The problem causes leakage of the air when actuating the robot and thus reducing the maximum pressure which can be generated inside of the actuator, and correspondingly the maximum curvature. In addition, the problem results in increasing the degree of nonlinearity of the robot due to the corresponding dynamics added, which challenges the modeling and control process.
- *Challenge #2 - Layer Delamination*: The second limitation is the separation of the 3D printed layers at higher pressures of operation, specifically near to the sharp edges. We observed that the possibility of delamination increases when actuators are repeatedly cycled between 250kPa–300 kPa. The issue is due to the nature of FDM 3D printing which relies on the adhesion between layers. Accordingly, if the printing is not conducted using a high-quality printing system, the adhesion may drop and can result in fatigue-based delamination under high pressure.
- *Possible Solutions*: In order to reduce the severity of the mentioned limitations, the following measures were taken. For the issue of moisture, it is suggested to heat up the filament before printing at 45 °C for around 2.5 hours. This reduces the existence of moisture. There are several dehydration machines on the market that can be used for this purpose. It should be noted that it is not advisable to have the temperature during dehydration above 50 °C as it may result in changes in the mechanical property of the material. For the issue of delamination, it is suggested to avoid sharp edges and use extra material on the edges and corners of the actuator in the design to provide more support. The combination of the above-given methods significantly reduced the possibility of leakage. To provide an additional layer of protection, we suggest using a sealing adhesive layer which can be sprayed or used as a polish after Printing. We suggest several sealing techniques, as detailed in Table V.

TABLE V
SEALING METHODS AND RESULTS

Material	Process	Results	Note
M.E.K Substitution 90% + Solvent 10%	Dip & dry 0.5 hour, Dip & dry 2 hours, Dip & dry 24 hours	30-60% Surface leakage sealed	Time consuming, Dangerous chemical needed
Acetone 50% + Sealant 50%	Mix, paint on actuator and dry for 45 min	100% Surface leakage sealed	Dangerous chemical needed
Rubbery sealant spray	Spray rubber on actuator surface, dry for 20 min	100% Surface leakage sealed	Actuators lose flexibility
Nail polish	Paint actuator with nail polish and dry for 20 min	100% Surface leakage sealed	Easy, Fast, Cheap and No flexibility loss

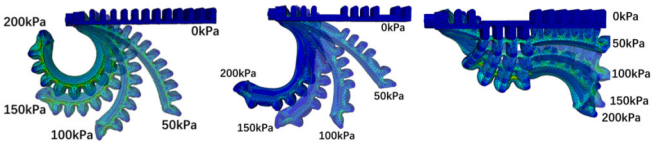

Fig. 4. Qualitative simulation results for the HH-Original, Flat and S-shape actuators, from left to right respectively.

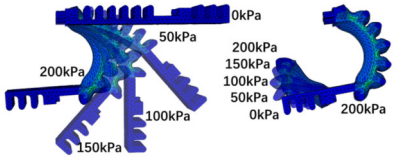

Fig. 5. Qualitative simulation results for 2DOF actuator.

D. Simulation of the Proposed Actuators

In this Section, Figs. 4 and 5 provide the simulation of various programmed soft robots based on the framework introduced. As can be seen in Figs. 4 and 5, different coding of the system can result in different shapes of the actuator. For the S-shape actuator given in Fig. 4, It can be seen that the use of both flexor-extensor bases resulted in generating two opposite curvatures. In Fig. 4, the gradual development of complex S-shape curvature can be seen with the increase of pressure from 0 kPa to 200 kPa. Regarding the 2DOF actuator designed with two independent air chambers shown in Fig. 5, it can be mentioned that the two chambers can be separately activated, resulting in a 2DOF serial mechanism. The 2DOF design is simulated under different pressurization conditions to illustrate achievable dexterity. First, Chamber 1 was pressurized with 200 kPa, while Chamber 2 carried 0 kPa. Then, Chamber 2 was pressurized, while Chamber 1 was kept at 200 kPa. When Chamber 1 is under 100 kPa pressure and Chamber 2 under 200 kPa pressure, the actuator showed a similar pose as a human thumb at a natural state, motivating the use in the context of soft bionic systems. We can see the gradual development of curvature along with increasing pressure. All actuators showed a high degree of dexterity. Through proper control of the pressure in the two Chambers, a variety of 2DOF curvatures and reaches can be generated.

E. Computational Evaluation

In order to evaluate the efficacy of the system, analyzing the linearity, hysteresis, and gradual behavior with respect to the pressure is important. We conduct a series of simulation-based

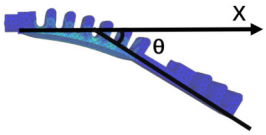

Fig. 6. Curvature angle θ definition.

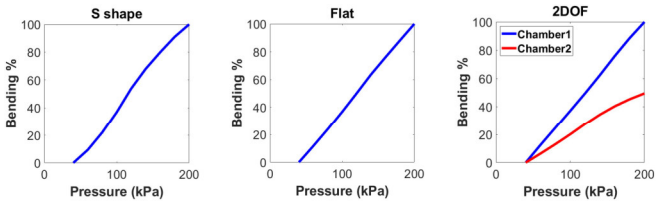

Fig. 7. Quantitative simulation results for S shape, Flat and 2DOF actuators in (a), (b) and (c) respectively

Fig. 8. 3D Printed Soft Robot Actuators.

and experiment-based measurements. Simulation-based evaluations are conducted to evaluate the change of the curvature, represented by angle θ. In this section, we show the performance of three chosen soft robots, given in Fig. 6. The results are shown in Fig. 7.

1) For flat actuator, R square value at 0.9995 shows a potentially-linear behavior. It should be noted that we expect to observe hysteresis loops and lower linearity when evaluating the system experimentally. By using simulation, we can gauge the potentials of the actuator.
2) S-shape actuator shows high linearity before 100 kPa. From 100 kPa to 200 kPa, the actuator showed a slower curvature growth due to activation of the extensor bases. Thus, extensor bases (if activated separately) may be used to control the rate of curvature increase.
3) For the 2DOF actuator, the deformation of 2 chambers was simulated individually. First, we keep Chamber 2 at 0 kPa and increase Chamber1 interior surface pressure. Then, we keep Chamber 1 at 0 kPa and pressurize Chamber 2. Both plots present good linearity with R square values at 0.9989 and 0.9789. Chamber 2 shows much lower growth which is due to the smaller size of the corresponding segment in the proposed design.

F. Experimental Implementation

Fig. 8 shows the 3D printed actuators with the optimized printing parameters (shown in Table IV), which resulted in an acceptable quality of printing in a relatively short time (3.5 hours per robot). Here we present the experimental observation on the performance of the three actuators under static and dynamic test settings. The actuators were activated between the minimum and maximum testing pressures (i.e., 40 kPa - 200 kPa). For the static test, the actuators were pressurized with an increment of 20 kPa discretely, while the recording was conducted at rest using a Goniometer sensor. For the dynamic test, the actuators were cycled continuously at a constant frequency when the sensor records the dynamical response of the actuator. The aforementioned settings allow for the examination of the behavior of the system, including the hysteresis of the actuator.

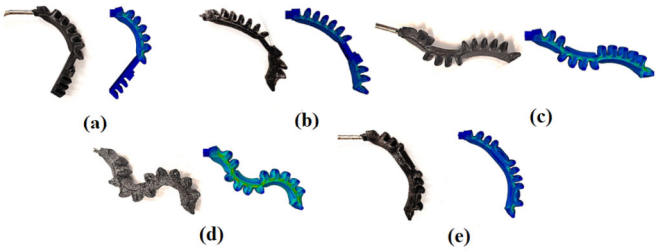

Fig. 9. Printed actuators and FEA qualitative verification.

IV. Results and Verification

A. 3D Printing and FEA Qualitative Verification

In order to qualitatively evaluate our 3D printed systems, the actuators were pressurized and compared with their simulation counterparts when inflated at the same intensity of pressure. Images of the actuator curvature are provided in Fig. 9. In Fig. 9(a), Chamber 1 of the printed 2DOF actuator is experimentally actuated at 100 kPa, and Chamber 2 is actuated at 0 kPa. The simulation result under similar pressure can be seen in Fig. 9(a). In Fig. 9(b), the shape of the printed 2DOF actuator can be seen when both chambers are experimentally actuated at 100 kPa. The simulation result can be seen in Fig. 9(b). Figs. 9(c) and 9(d) demonstrate the comparison for the S-shape actuator inflated at 100 kPa and 200 kPa, respectively. Also, Fig. 9(e) shows the comparison for the flat actuator at 100 kPa. Based on the results shown in Fig. 9, it can be visually seen that the 3D printed actuator showed similar curvature to the corresponding FEA results. The results support that the overall behavior of the actuators follows the expected behavior from the simulation. This is the qualitative evaluation which, in combination with our quantitative evaluation (Section IV.B), highlights the performance of the printed actuator in comparison to the FEA simulation.

B. 3D Printing and FEA Quantitative Verification

We have conducted two sets of experiments, one under static pressure (when we increase the input pressure stepwise and waited for any transient motion to pass) and once when we evaluate the performance of the actuator through dynamic pressurizing to highlight the dynamic hysteresis behavior. Figs. 10 and 11 include experimental results for the static and dynamic tests. Each trace shows one cycle of pressurizing.

The experimental setup is developed by our team, which has four positive controllable pressure outputs and four negative controllable pressure outputs. The system is controlled in MATLAB

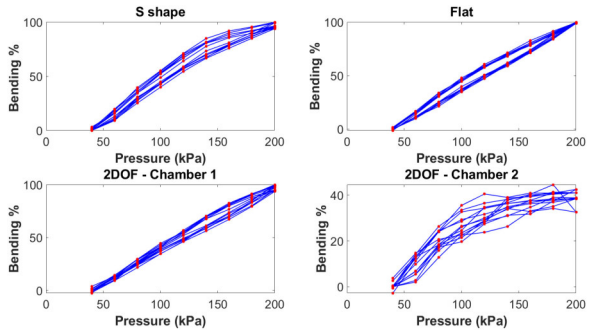

Fig. 10. Static pressure test plots.

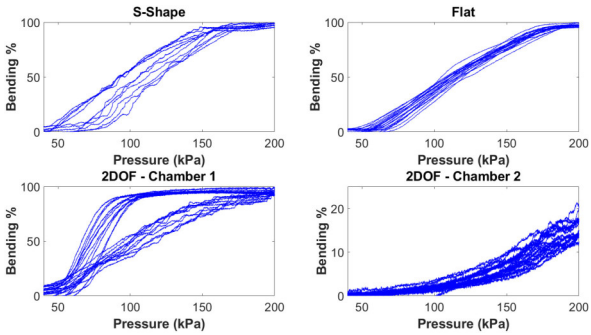

Fig. 11. Dynamic pressure test plots.

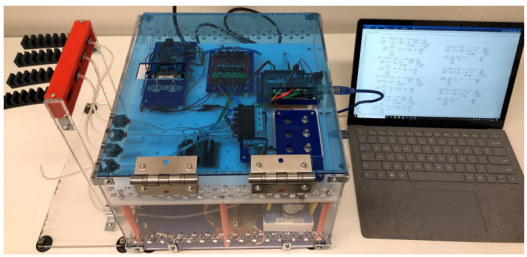

Fig. 12. Soft robot control station.

using the QUARC Realtime library by (Quanser Inc. Canada). The setup is shown in Fig. 12.

The experimental data were collected with the Delsys Wireless Trigno Digital Goniometer, in real-time, and recorded by Delsys software. The goniometer modules are placed into two white hubs at the ends of the actuators to fixate the Goniometer to the body of the actuator. The first module is placed over the air input port of the actuators and acted as an angular reference for the second module, which is placed at the endpoint of the actuator for recording the angle when the actuator is bending. The measurement system used in the experiments is given in Fig. 13.

For the static test, we cycle the pressure slowly from 40 kPa to 200 kPa and backward, with 8 static increments of 20 kPa. After each increment or decrement, when the actuator's angle was at a steady-state, we recorded the deflection value with the digital Goniometer. We repeated this oscillatory process 10 times for 3 actuators. For the dynamic test, we increased and decreased the

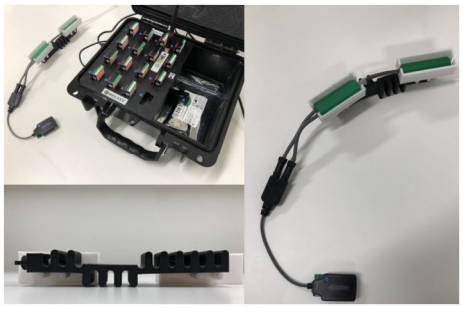

Fig. 13. The measurement system using Delsys Goniometer used for the experiments.

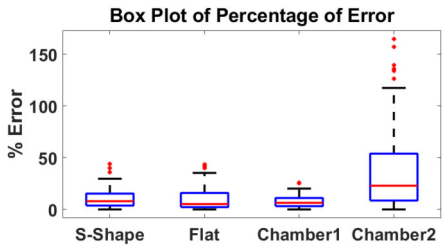

Fig. 14. Boxplots of differences between simulation and experiments.

TABLE VI
BOXPLOT DATA

	S Shape	Flat	Chamber 1	Chamber 2
Standard Deviation	8.31%	11.31%	5.56%	40.72%
Mean	10.36%	10.29%	7.50%	38.36%
Median	7.99%	5.18%	6.42%	22.92%
Minimum	0%	0%	0%	0%
Maximum	43.94%	43.59%	25.80%	164.88%

pressure continuously 10 times for all 3 actuators. The results are normalized for comparison between different actuators. Figs. 10 and 11 show the normalized results of the static and dynamic test, respectively.

In Fig. 10, the red dots are discrete angles recorded after each separate static actuation when the actuators have reached a steady state. The blue trace connects the red dots to show the overall pattern and highlight the inherent hysteresis in the system. In Fig. 11, the blue traces show the response of the actuator to the continuous dynamic pressure change. As expected, we observed that the results from the dynamic test are different from static results, as we see higher nonlinearity and larger hysteresis in the system due to excitation of internal dynamics of the system, which are not observed in the static test. In other words, the dynamic behavior is affected by the pneumatic delay, which does not allow the actuators to inflate and deflate completely during dynamical cycles, which results in higher hysteresis.

In addition to the above, to quantitatively evaluate the performance of the implemented actuators, the deviation between simulation and static experiments are plotted using box plots (Fig. 14), and the corresponding statistical results are given in Table VI. As can be seen, the flat actuator and chamber 1 of the 2DOF actuator have the least deviation from the simulation,

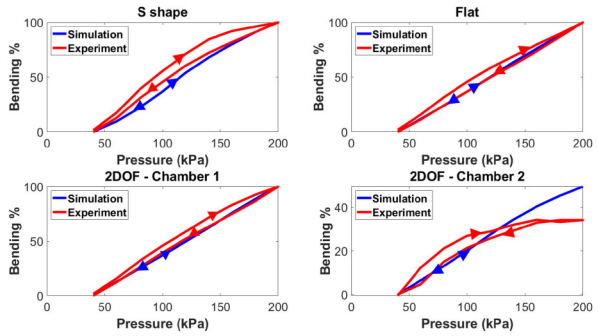

Fig. 15. Static tests compared to FEA quantitative results.

which is due to the low hysteresis behavior, while chamber 2 of the 2DOF actuator shows the largest error. The objective values are given in Table VI.

The qualitative and quantitative experimental results verified our design and illustrated the potential of this new family of soft actuators. At the same time, the hysteresis of the actuator highlights the need for a powerful and robust close loop control. This forms our future line of work. In addition, to compare the experimental and simulation results for the static test, we computed the averaged hysteresis behavior of each actuator and compared it with the simulation results. The reason for choosing the static test is that the designed FEA simulation does not model the dynamical behavior of the system. In Fig. 15, the arrows show the direction of actuation when upward means increment of pressure and downward means decrements of pressure. Fig. 15 compares the corresponding simulation and experiments.

As can be seen in Fig. 15, the major difference between the simulation and the experimental result is the hysteresis behavior, which is not modeled in FEM and causes a discrepancy between the simulated and experimental performance, as expected. The result highlights the significance of hysteresis, which should be taken into account when designing advanced control algorithms for delicate tasks. We also observed that the S-shape actuator and the second chamber of the 2DOF actuator show lower compliance with the simulation due to large hysteresis. We believe the reason is due to the complexity of the shape and the smaller length of the active segments. In contrast, the flat actuator and the first chamber of the 2DOF actuator have lower hysteresis and more compliance with the simulation results.

V. Conclusion and Future Work

In this paper, we proposed the concept of the structurally programmable soft robot using a novel design of the 3D printable mechanical library and embedded functions to be implemented on the backbone structure for programming the robot. We have shown that through structural coding, it is possible to generate a wide range of continuum robots. We also showed that the system has the potential to be scaled up for multiple DOF, while the dexterity and range can be structurally programmed. The results open doors for a variety of novel complex soft continuum robots with specific applications in the medical domain. One future line of work will be focused on a comprehensive study on the dynamical behavior of the robot and the closed-loop control.

In this paper, we focus on the design and validation of the proposed mechanically-programmable framework and experimentally evaluate their response behavior to static and dynamic pressure. In this paper, we do not analyze the force capability, as well as the incorporation of gravity in the simulation and experimental settings. This paper provides a framework to design and implement different soft actuators using the proposed "mechanical library" and "embedded functions." The proposed library can be expanded to include more embedded mechanical functions for producing various soft actuators and robots. The future line of research will include evaluation of the force capacity and closed-loop control using our soft-robot station (Fig. 12).

References

[1] J. Kwon *et al.*, "Flat inflatable artificial muscles with large stroke and adjustable force-length relations," *IEEE Trans. Robot.*, vol. 36, no. 3, pp. 743–756, Jun. 2020.
[2] M. Koehler *et al.*, "Model-based design of a soft 3-D haptic shape display," *IEEE Trans. Robot.*, vol. 36, no. 3, pp. 613–628, Jun. 2020.
[3] T. Hainsworth *et al.*, "A fabrication free, 3D printed, multi-material, self-sensing soft actuator," *IEEE Robot. Automat. Lett.*, vol. 5, no. 3, pp. 4118–4125, Jul. 2020.
[4] S. F. Atashzar *et al.*, "Review: How can intelligent robots and smart mechatronic modules facilitate remote assessment, assistance, and rehabilitation for isolated adults with Neuro-Musculoskeletal conditions?,"*Front Robot AI*, vol. 8, Apr. 2021, Art. no. 610529.
[5] T. Shahid *et al.*, "Moving toward soft robotics: A decade review of the design of hand exoskeletons," *Biomimetics*, vol. 3, no. 3, 2018, Art no. 17, doi: 10.3390/biomimetics3030017.
[6] S. K. Powell *et al.*, "Past, present, and future of soft-tissue prosthetics: Advanced polymers and advanced manufacturing," *Adv. Mater.*, vol. 32, no. 42, p. 2001122, 2020.
[7] M. J. B. Enojas and M. C. Ramos, "Development of a finger soft pneumatic bending actuator," in *Proc. 4th Asia-Pacific Conf. Intell. Robot Syst.*, 2019, pp. 1–5.
[8] C. Chen *et al.*, "Fiber-reinforced soft bending actuator control utilizing on/off valves," *IEEE Robot. Automat. Lett.*, vol. 5, no. 4, pp. 6732–6739, Oct. 2020.
[9] J. Bishop-Moser and S. Kota, "Design and modeling of generalized fiber-reinforced pneumatic soft actuators," *IEEE Trans. Robot.*, vol. 31, no. 3, pp. 536–545, Jun. 2015.
[10] R. Deimel and O. Brock, "A novel type of compliant and underactuated robotic hand for dexterous grasping," *Int. J. Robot. Res.*, vol. 35, no. 1–3, pp. 161–185, 2016.
[11] J. S. Khan *et al.*, "Actuation and fabrication of human inspired artificial hand," in *Proc. 4th Int. Conf. Inf. Syst. Comput. Netw.*, 2019, pp. 315–320.
[12] J. M. Florez *et al.*, "Soft pneumatic actuators for legged locomotion," in *Proc. IEEE Int. Conf. Robot. Biomimetics*, 2014, pp. 27–34.
[13] C. Premarathna *et al.*, "A novel fabrication method for rapid prototyping of soft structures with embedded pneumatic channels," in *Proc. Moratuwa Eng. Res. Conf.*, 2019, pp. 430–435.
[14] A. Al-Ibadi *et al.*, "A circular pneumatic muscle actuator (CPMA) inspired by human skeletal muscles," in *Proc. IEEE Int. Conf. Soft Robot.*, 2018, pp. 7–12.
[15] W. Hu *et al.*, "3D printed helical soft pneumatic actuators," in *Proc. IEEE/ASME Int. Conf. Adv. Intell. Mechatronics*, 2018, pp. 950–955.
[16] H. K. Yap *et al.*, "High-force soft printable pneumatics for soft robotic applications," *Soft Robot.*, vol. 3, no. 3, pp. 144–158, 2016.
[17] C. Tawk *et al.*, "Position control of a 3D printed soft finger with integrated soft pneumatic sensing chambers," in *Proc. 3rd IEEE Int. Conf. Soft Robot.*, 2020, pp. 446–451.
[18] K. Zhang *et al.*, "A design and fabrication approach for pneumatic soft robotic arms using 3D printed origami skeletons," in *Proc. 2nd IEEE Int. Conf. Soft Robot.*, 2019, pp. 821–827.
[19] C. Tawk *et al.*, "A 3D-printed omni-purpose soft gripper," *IEEE Trans. Robot.*, vol. 35, no. 5, pp. 1268–1275, Oct. 2019.

[20] C. Tawk *et al.*, "Fully 3D printed monolithic soft gripper with high conformal grasping capability," in *Proc. IEEE/ASME Int. Conf. Adv. Intell. Mechatronics*, 2019, pp. 1139–1144.
[21] L. Rosalia *et al.*, "Geometry-based customization of bending modalities for 3D-printed soft pneumatic actuators," *IEEE Robot. Automat. Lett.*, vol. 3, no. 4, pp. 3489–3496, Oct. 2018.
[22] N. Wang *et al.*, "A kind of soft pneumatic actuator based on multi-material 3D print technology," in *Proc. IEEE Int. Conf. Robot. Biomimetics*, 2017, pp. 823–827.
[23] B. W. Ang and C.-H. Yeow, "Print-it-yourself (PIY) glove: A fully 3D printed soft robotic hand rehabilitative and assistive exoskeleton for stroke patients," in *Proc. IEEE/RSJ Int. Conf. Intell. Robots Syst.*, 2017, pp. 1219–1223.
[24] Y. Yang and Y. Chen, "Novel design and 3D printing of variable stiffness robotic fingers based on shape memory polymer," in *Proc. 6th IEEE Int. Conf. Biomed. Robot. Biomechatronics*, 2016, pp. 195–200.
[25] T. Kalisky *et al.*, "Differential pressure control of 3D printed soft fluidic actuators," in *Proc. IEEE/RSJ Int. Conf. Intell. Robots Syst.*, 2017, pp. 6207–6213.
[26] O. D. Yirmibesoglu *et al.*, "Direct 3D printing of silicone elastomer soft robots and their performance comparison with molded counterparts," in *Proc. IEEE Int. Conf. Soft Robot.*, 2018, pp. 295–302.
[27] B. N. Peele *et al.*, "3D printing antagonistic systems of artificial muscle using projection stereolithography," *Bioinspiration Biomimetics*, vol. 10, no. 5, p. 055003, Sep. 2015.
[28] D. B. Comber *et al.*, "Design, additive manufacture, and control of a pneumatic MR-compatible needle driver," *IEEE Trans. Robot.*, vol. 32, no. 1, pp. 138–149, Feb. 2016.
[29] J. E. Slightam and V. R. Gervasi, "Novel integrated fluid-power actuators for functional end-use components and systems via selective laser sintering nylon 12," in *Proc. 23rd Ann. Int. Solid Freeform Fabr. Symp*, 2012, pp. 197–211.
[30] A. Rost and S. Schädle, "The SLS-generated soft robotic hand-an integrated approach using additive manufacturing and reinforcement learning," in *Proc. 12th Int. Conf. Mach. Learn. Appl.*, 2013, vol. 1, pp. 215–220.
[31] A. Grzesiak *et al.*, "The bionic handling assistant: A success story of additive manufacturing," *Assembly Automat.*, vol. 31, no. 4, pp. 329–333, Jan. 2011.
[32] R. MacCurdy *et al.*, "Printable hydraulics: A method for fabricating robots by 3D co-printing solids and liquids," in *Proc. IEEE Int. Conf. Robot. Automat.*, 2016, pp. 3878–3885.
[33] A. D. Marchese and D. Rus, "Design, kinematics, and control of a soft spatial fluidic elastomer manipulator," *Int. J. Robot. Res.*, vol. 35, no. 7, pp. 840–869, 2016.
[34] Y. Yang *et al.*, "Bioinspired robotic fingers based on pneumatic actuator and 3D printing of smart material," *Soft Robot.*, vol. 4, no. 2, pp. 147–162, 2017.
[35] F. Connolly *et al.*, "Mechanical programming of soft actuators by varying fiber angle," *Soft Robot.*, vol. 2, no. 1, pp. 26–32, 2015.
[36] B. Treml *et al.*, "Origami mechanologic," in *Proc. Nat. Acad. Sci. USA*, vol. 115, no. 27, pp. 6916–6921, 2018.
[37] Y. Song *et al.*, "Additively manufacturable micro-mechanical logic gates," *Nature Commun.*, vol. 10, no. 1, pp. 1–6, 2019.
[38] A. K. Mishra *et al.*, "Autonomic perspiration in 3D-printed hydrogel actuators," *Sci. Robot.*, vol. 5, no. 38, 2020, doi: 10.1126/scirobotics.aaz3918.
[39] J. Horvath and R. Cameron, *Mastering 3D Printing*. Berlin, Germany: Springer, 2020.